

# Optimizing Reconfigurable Intelligent Surfaces in Multi-User Environments: A Multiport Network Theory Approach Leveraging Statistical CSI

Andrea Abrardo *Senior Member, IEEE*

**Abstract**—Reconfigurable Intelligent Surfaces (RIS) are one of the emerging technologies aimed at meeting the expectations of next-generations wireless systems. In this field, the use of multiport network models for the characterization and optimization of RIS has emerged in recent years. These models take into account aspects traditionally not considered in communication theory, such as mutual coupling of RIS elements and the presence of structural scattering. In this work, we refer to this model and focus on the problem of maximizing the average achievable rate in a multi-user uplink scenario by leveraging statistical Channel State Information (CSI). This approach significantly reduces the computational burden and communication overhead in CSI estimation compared to schemes requiring instantaneous CSI estimation. These benefits are achieved with performance that, in many cases, is reasonably close to that of the perfect CSI scenario. This is one of the outcomes achievable with the proposed optimization scheme. Moreover, it is shown how in multi-user scenarios, namely in the presence of interference, the use of inadequate models to characterize RIS can lead to very poor performances. For example, models that do not consider structural scattering may fail to account for interference caused by RIS.

**Index Terms**—Reconfigurable intelligent surface, Multi-user uplink communications, structural scattering, mutual coupling, statistical CSI, optimization.

## I. INTRODUCTION

Reconfigurable Intelligent Surfaces (RIS) are considered a promising technology in the context of next-generation wireless systems, particularly those operating at mmWave frequencies or even higher [1]–[3]. The use of RIS for supporting communications in a cellular scenario primarily aims to boost system capacity or to aid communications with nodes in poor connection conditions with the base station (BS). This issue is well known in cellular systems and can traditionally be addressed through the aid of additional BSs deployed specifically to increase system capacity, for example, mounted on UAVs, or through the use of Coordinated multipoint (CoMP) transmissions, where two BSs coordinate to transmit to a single ‘unlucky’ user, positioned, for example, at the cell edge [4]–[7]. The fundamental difference between the two approaches is that RIS are essentially passive structures that can only reflect a signal transmitted by another transmitter and cannot perform beamforming towards a node themselves.

A. Abrardo is with the University of Siena and CNIT, Italy (e-mail: [abrardo@unisi.it](mailto:abrardo@unisi.it)). The work is supported by the 6G SHort range extreme communication IN Entities (SHINE) European project. I would like to express my sincere gratitude to Professors Marco Di Renzo and Alberto Toccafondi for their invaluable contributions to this work. The collaboration with Marco Di Renzo in several past and present research activities in the field of RIS modeling and optimization has been instrumental in shaping the direction of this research. The support of Alberto Toccafondi allowed to enrich my understanding and expertise in electromagnetic modeling.

In this sense, RIS are more properly seen as part of the propagation environment, realizing the concept of a *smart radio environment*. In this case, the wireless system goes beyond conventional communication device parameters, with the environment itself, e.g., the channel, becoming a variable that can be optimized. Besides the undeniable advantages in terms of cost and power consumption, RIS introduce a series of new challenges compared to traditional MIMO systems, such as the problem of channel estimation.

Indeed, in RIS-aided communications, estimation of the cascaded channel from the User Equipment (UE) to RIS and from the RIS to the BS, is essential for effective phase-shift design and harnessing the benefits offered by RIS technology. However, this task is complex, mainly due to the passive characteristics of the RIS and the complexities posed by high-dimensional channels [8]–[10]. Indeed, since all RIS elements are passive and cannot transmit, receive, or process any pilot signals, Channel State Information (CSI) estimation must be performed by a central controller, such as the BS. This incurs significant overhead compared to standard MIMO systems, as it requires substantial resources to estimate the channel.

Another aspect that differentiates RIS from traditional MIMO systems is the structural limitation that they are only capable of reflecting an incident signal. To this respect, in the majority of works addressing RIS optimization for communications and/or CSI estimation, a RIS is characterized as a planar array comprising a given number of reflective elements strategically positioned at sub-wavelength intervals. The impedance of each element can be finely adjusted to introduce a controllable phase-shift to the incident wave before reflecting it. By optimizing the phase-shift pattern across the RIS, it becomes possible to manipulate the reflected wavefront, directing it into a beam aimed at the intended receiver. These models are not always electromagnetically consistent, since they do not consider several aspects that play an important role in characterizing the operation of a realistic RIS [11], [12]. Recent results highlight, in fact, the critical need of using realistic reradiation models, which result in a strong interplay between the surface-level optimization of RISs and the element-level design of the RIS elements [13]. In this context, multiport network theory has been proved to be a suitable approach for modeling and optimizing RIS-aided channels [14]–[19]. In two recent works [20], [21], an easily applicable MP network model is proposed, based on the  $S$  and  $Z$  parameters representation of the network. This model reveals the approximations inherently considered in classical RIS models used in communication theory that assume the RIS as an ideal scatterer.

Specifically, the classical RIS models overlook the effects of: (i) electromagnetic mutual coupling between scattering elements; (ii) correlation between the phase and amplitude of the reflection coefficient; (iii) the presence of a structural scattering component, leading to an unwanted specular component of the reflected wavefront. Multi-port network models, on the other hand, allow these aspects to be incorporated into an easily manageable end-to-end model. This model enables optimizations that account for all scattering components. For example, with regard to the structural scattering component, disregarding it may result in unwanted interference, which a multi-port network model-based optimizer can easily eliminate. This effect, in particular, will be demonstrated in the results presented in this work, along with showing the effect of mutual coupling in the characterization of the RIS's response. In all these works dealing with multiport network models, the channel is assumed to be perfectly known at the central controller, and RIS optimization is carried out accordingly. On the other hand, many works in the literature consider the channel estimation problem when RIS are characterized with classical models where each element is a pure phase shifter. Specifically, research in this field has so far pursued two main approaches. On one hand, known as *Single time-scale CSI and RIS optimization*, methods have been developed to facilitate instantaneous channel estimation. This is achieved by transmitting pilot signals and subsequently configuring the RIS based on predetermined patterns at a timescale matching the channel coherence time. In this vein, approaches such as those in [22]–[25] aim to minimize the number of pilot symbols, while approaches in [26], [27] address the same problem in the presence of electromagnetic interference. A diagram summarizing this type of approaches is shown in Fig. 1 (a). In this case, the necessity to configure the RIS multiple times before obtaining reliable CSI could greatly diminish their advantages. This is particularly true if the number of individually reconfigurable elements is excessively large or if an inefficient channel estimation algorithm is employed [28], [29]. Furthermore, considering the dynamic nature of the wireless channel and user mobility, optimizing a RIS within a timescale aligned with the coherence time of the channel can be challenging. This is especially true in highly dynamic environments [2].

To address these open research issues, another approach proposed in the literature does not strictly depend on perfect CSI knowledge for RIS optimization. See, for example, [28], [30]–[33]. In particular, the RIS is optimized based on the statistical CSI of all links, which operates on a long time-scale, effectively reducing the CSI overhead. Estimation of the statistical CSI can be conducted through large time-scale sensing, as proposed in [30], or by leveraging localization information, as suggested in [31]. These approaches can be referred to as *Two-time-scale CSI and RIS optimization* and are summarized in Fig. 1 (b). These schemes involve a two-phase optimization process. The first phase is offline, which is long-term and sporadic. The second phase is online, which is short-term and more frequent. During the online phase, communication between the BS and the UEs is optimized without interaction with the RISs. The key advantage of this

approach is that the RIS can be optimized without the need for repeated reconfigurations with predetermined patterns. Furthermore, the information necessary for RIS optimization can be obtained sporadically. This information may be known beforehand, such as knowledge of UEs confined to a specific area. It can also be learned occasionally during system operation, using a localization infrastructure.

#### A. Contribution

We consider a MP network model for RIS that addresses several factors often overlooked by traditional RIS models in communication theory. These include the mutual coupling among scattering elements and the presence of structural scattering.

The MP model, which allows for a more realistic characterization of the RIS in a communication system compared to traditional models, does indeed have the drawback of featuring a nonlinear transfer function. Previous studies enhancing the MP model have assumed perfect knowledge of the channel at the central controller, and RIS optimization has been conducted accordingly. In contrast, this paper addresses the CSI problem and considers a scenario where RIS optimization is performed solely based on second-order CSI statistics, as outlined in the scheme shown in Figure 1 (b). In this context, to solve the problem, we proceed as follows:

- First, we establish the equivalence between the problem of maximizing the mean rate subject to interference, which is our primary problem, and an LMMSE estimation problem, which we define as the dual problem.
- The dual problem involves the introduction of an auxiliary variable in the primal problem, leading to its decomposition into multiple manageable subproblems.
- We leverage the linearization of the transfer function of the RIS to address the RIS optimization sub-problem.
- Finally, we employ an alternating optimization approach to obtain a local maximum of the primal problem.

To the best of our knowledge, this is the first work in which the MP network model is used in a multi-user scenario where there is no perfect CSI.

The analysis and RIS optimization strategy proposed in this paper are general and do not depend on a specific approach for channel correlation estimation. Nevertheless, in the Results Section, we present results for a case in which the correlation matrix is estimated from location information.

The RIS optimization proposed in this paper is carried out assuming that in the channel between the BS and the RIS, the presence of natural scattering can be neglected and that the BS and the RIS are positioned in fixed and known locations. The first assumption arises from the consideration that the BS and the RIS can, in many cases, be optimally deployed to have a very strong Line-of-Sight (LOS) component. However, in the model considered for simulations, we will take into account the presence of multipath also in the BS-RIS link.

In the Results section, we will demonstrate the validity of the proposed approach. It will be shown that, although the absence of perfect CSI inevitably results in performance degradation compared to the ideal perfect CSI case, the performance gap is often not substantial. This justifies the

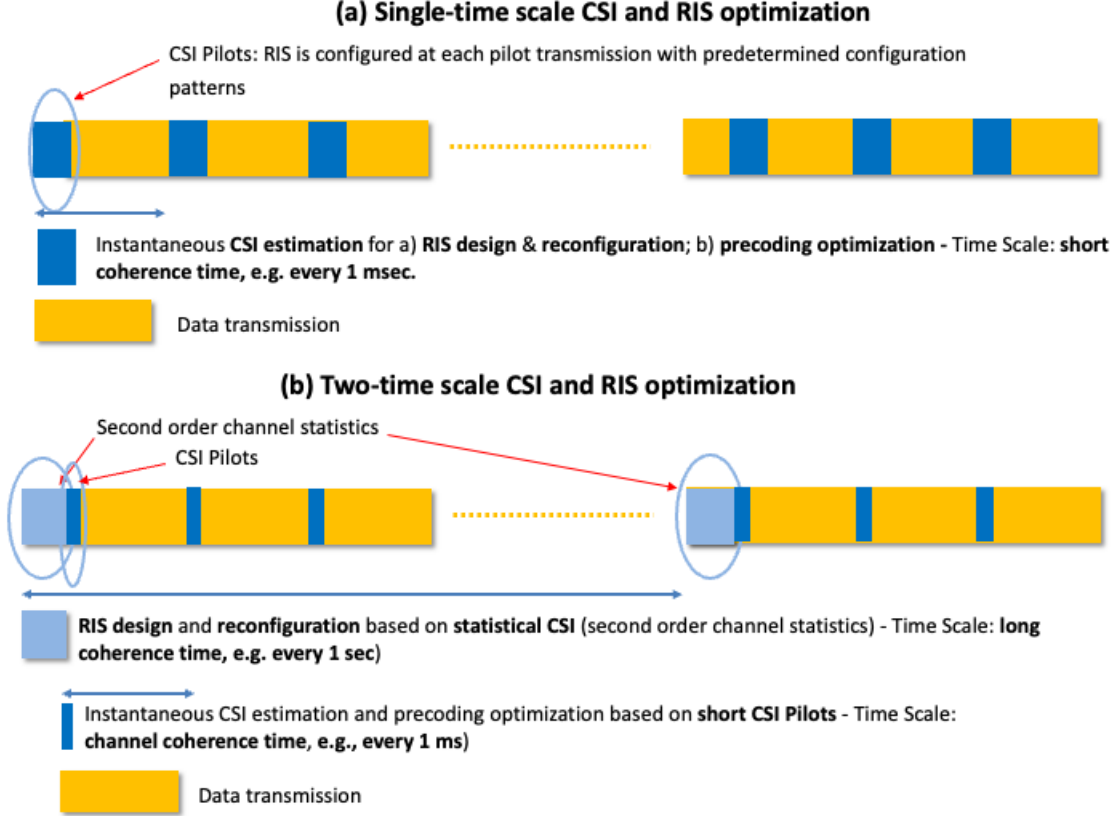


Fig. 1: Possible approaches for RIS optimization.

adoption of approaches based on statistical CSI due to their reduced complexity and overhead. Moreover, it is shown how in multi-user scenarios, particularly in the presence of interference, the use of inadequate models to characterize RIS can lead to very poor performance. For example, models that do not consider structural scattering may fail to account for interference caused by RIS.

### B. Paper Outline and Notation

The rest of this paper is organized as follows. In Section II, we introduce the model adopted for the system. In Section III, the MP network model for the RIS characterization is proposed. In Section IV, we provide an iterative algorithm with provable convergence that allows carrying out the RIS optimization. Numerical results are presented in Section V, while conclusions are drawn in Section VI.

*Notation:* Unless otherwise specified, matrices are denoted by bold uppercase letters (i.e.,  $\mathbf{X}$ ), vectors are represented by bold lowercase letters (i.e.,  $\mathbf{x}$ ), and scalars are denoted by normal font (i.e.,  $x$ ).  $(\cdot)^T$ ,  $(\cdot)^H$  and  $(\cdot)^{-1}$  stand for the transpose, Hermitian transpose and inverse of the matrices. The symbol  $\odot$  represents the Hadamard (element-wise) product while with  $\text{diag}(\mathbf{x})$  we mean the diagonal matrix obtained from the element of vector  $\mathbf{x}$  and with  $\text{diag}(\mathbf{X})$  the vector obtained from the diagonal matrix of  $\mathbf{X}$ . The notation  $\|\mathbf{x}\|$  signifies the Euclidean norm of the vector  $\mathbf{x}$ ,  $\|\mathbf{X}\|$  is the Frobenius norm of the matrix  $\mathbf{X}$ , and  $\mathbb{E}\{\cdot\}$  represents the statistical expectation. Finally,  $\mathbf{I}_n$  indicates the identity matrix of dimension  $n$ .

## II. SYSTEM MODEL

We consider a wireless scenario where a single-antenna UE must establish a communication link with an  $N$ -element BS. The BS antennas are arranged in a uniform planar array (UPA) with  $N_H$  rows and  $N_V$  columns, resulting in  $N = N_H N_V$ . In this environment, a RIS is present with the goal of supporting the communication of the intended UE, while  $N_u - 1$  users are also present and act as interferers for that node. We are particularly interested in studying the capabilities of the RIS to improve the link quality of the intended UE while simultaneously limiting the interference from other UEs. This analysis is conducted with only statistical knowledge of the channel to all the involved nodes. The reference scenario is, for example, one in which the interfering nodes are communicating with another BS or with the same BS without the aid of the RIS, or with the aid of a different RIS.

The RIS is equipped with  $M$  passive reconfigurable elements, forming a UPA with  $M_H$  rows and  $M_V$  columns, where  $M = M_H M_V$ . Without loss of generality, we assume that the first UE serves as the reference user. Hence, in the considered scenario, the objective of the RIS is to maximize the rate of the first UE, while users  $i$ , where  $i = 2, \dots, N_u$ , act as interferers.

A graphical representation of the scenario is shown in Fig. 2. The channels connecting the UE  $i$  with the RIS and the BS are denoted by  $\mathbf{t}_i \in \mathbb{C}^{M \times 1}$  and  $\mathbf{p}_i \in \mathbb{C}^{N \times 1}$ , respectively. Additionally,  $\mathbf{S} \in \mathbb{C}^{N \times M}$  represents the channel between the RIS and the BS. For the direct links  $\mathbf{p}_i$ , we assume that only the Non-Line-Of-Sight (NLOS) components due to natural

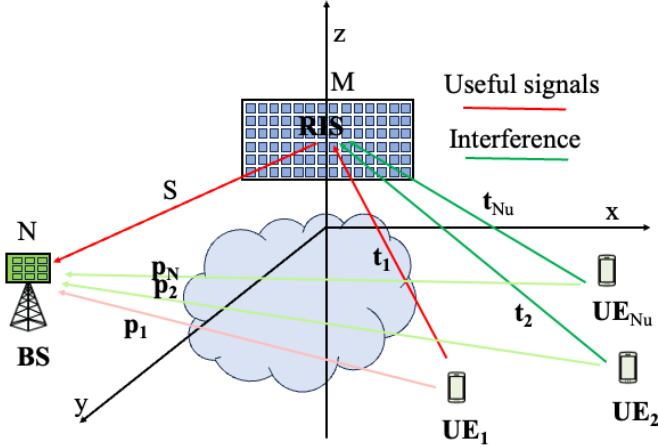


Fig. 2: RIS-aided communication system.

scattering are received at the BS, which is the situation where the use of RIS can be beneficial. We can express the received vector  $\mathbf{y} \in \mathbb{C}^{N \times 1}$  as follows:

$$\mathbf{y} = \left( \mathbf{S} \Delta(\mathbf{z}) \sum_{i=1}^{N_u} \mathbf{t}_i + \sum_{i=1}^{N_u} \mathbf{p}_i \right) s_i + \mathbf{n}. \quad (1)$$

Here,  $\Delta(\mathbf{z}) \in \mathbb{C}^{M \times M}$  is the RIS reflecting matrix, dependent on a vector  $\mathbf{z} \in \mathbb{C}^{M \times 1}$  of tunable parameters,  $s_i$  represents the transmitted symbol by UE  $i$  with transmitted power  $\mathbb{E}(|s_i|^2) = \sigma_i^2$ , and  $\mathbf{n} \in \mathbb{C}^{N \times 1}$  is the thermal noise with variance  $\sigma_n^2$ .

The BS estimates the transmitted signal  $s_1$  by using the combining vector  $\mathbf{v} \in \mathbb{C}^{N \times 1}$  to obtain  $\hat{s}_1 = \mathbf{v}^H \mathbf{y}$ .

### III. RIS MODELS

#### A. MP Model

By referring to the MP  $Z$ -parameters representation of an end-to-end channel matrix involving an RIS as presented in [20], we obtain:

$$\Delta_{MP}(\mathbf{z}) = -2Y_0(\mathbf{Z}_{SS} + r_0 \mathbf{I}_M + \mathbf{Z}_R)^{-1}. \quad (2)$$

Here,  $\mathbf{Z}_{SS} \in \mathbb{C}^{M \times M}$  denotes the matrix of self and mutual impedances of the RIS,  $\mathbf{Z}_R = \text{diag}(\mathbf{z})$ , where  $\mathbf{z} = j\mathbf{b}$  are tunable impedances connected at the RIS ports,  $r_0$  represents a small parasitic resistance,  $\mathbf{I}_M$  stands for the identity matrix, and  $Y_0$  is a reference admittance defined as:

$$Y_0 = \frac{Z_0}{(Z_0 + Z_{RR})(Z_0 + Z_{TT})}. \quad (3)$$

In (3),  $Z_0$  is the reference impedance across which the transmitter and receiver ports are terminated, while  $Z_{RR}$  and  $Z_{TT}$  denote the self-impedances of the receiver and transmitter ports. For simplicity, it is assumed that  $Z_0$  is uniform across all ports and equals to  $Z_0 = 50 \Omega$ . Note that (2) has dimensions of  $\Omega^{-2}$ , consistent with the  $Z$ -parameter representation of the multiport, where  $\mathbf{S}$  and  $\mathbf{t}_i$  in (1) denote impedance matrices with dimensions of  $\Omega$ . The values of  $\mathbf{Z}_{SS}$ ,  $Z_{RR}$ , and  $Z_{TT}$  can be analytically computed as demonstrated in [15], or determined using full-wave simulators as shown in [20], [21]; nevertheless, they can be assumed to be known since they rely

on the structural characteristics of the RIS, such as the length and spacing between dipoles (in the case of RIS composed of dipoles).

#### B. Communication Theory (CT) Model

In order to characterize a RIS within a communication system, including UEs and BSs, it is customary to represent it as surfaces composed of ideal scatterers capable of imparting a phase shift on the impinging signal. This model, which we will refer to as the Communication Theory model (CT) hereafter, can be represented by a diagonal reflection matrix with elements:

$$[\Delta_{CT}]_{m,m} = J_0 \Gamma_m \quad (4)$$

where  $J_0$  is a constant depending on the geometry of the scatterer, and  $\Gamma_m = e^{j\phi_m}$  is the load reflection coefficient with  $0 \leq \phi_m \leq 2\pi$ .

#### C. Comparison between CT and MP models

The CT model in (4) can be seen as a particular case of the more general MP model in (2), as broadly discussed in [20]. It is indeed straightforward to derive the CT model from the MP one by making the following assumptions. First we neglect the parasitic resistance  $r_0$  and impose  $\mathbf{Z}_{SS} = Z_0 \mathbf{I}_M$ . In this manner, beyond ignoring the mutual coupling, the scattering matrix of the RIS becomes zero, and the effect of the RIS is solely to introduce a pure phase shift to the incident signal. This simplified model is denoted by ideal Multi-Port (iMP) which, from (2), yields a diagonal RIS reflection matrix with elements:

$$[\Delta_{iMP}(\mathbf{b})]_{m,m} = -2Y_0(Z_0 + jb_m)^{-1}. \quad (5)$$

Hence, it is easy to verify that:

$$\Delta_{iMP}(\mathbf{b}) = \Delta_{CT} - \frac{Y_0}{Z_0} \mathbf{I}_M, \quad (6)$$

when  $J_0 = \frac{Y_0}{Z_0}$  and

$$\Gamma_m = \frac{jb_m - Z_0}{jb_m + Z_0} \quad (7)$$

in (4). The above equation allows to shed light on a third important approximation which is inherent in the CT model, in which  $\Delta_{\mathbf{S}} = -\frac{Y_0}{Z_0} \mathbf{I}_M$  is not considered. This term corresponds to the scattered signal obtained when the RIS is terminated with impedances  $z_m = Z_0$ , i.e., when the load reflection coefficient is zero, and hence the CT model would entails zero scattered energy. This structural component causes the RIS to behave like a scatterer that does not introduce any phase shift on the incident signal, thereby introducing a specular component that, as we will see, cannot be ignored without significantly deteriorating performance in certain situations.

### IV. RIS OPTIMIZATION

#### A. Problem Formulation

For RIS optimization purposes, we do not consider the direct links  $\mathbf{p}_i$  between the UEs and the BS, as these links are not under the control of the RIS. On the other hand, as discussed in most previous works on RIS (e.g., see [28], [34],

[35]), in the presence of a strong BS-UE direct link, the impact and contribution of the RIS are usually not very significant. Hence, optimizing the RIS to account for this possibility typically provides no significant benefit. It should also be noted that in the presence of a direct link, the optimization of the RIS should be able to coherently combine its reflected contribution with the direct one at the receiver, which can only be done with a perfect channel estimation. Therefore, in the scenario of only statistical channel knowledge, the RIS can be optimized considering only the contribution of the reflected path. The presence of the direct path will nonetheless be considered in the Results section.

To elaborate, since  $\mathbf{z} = j\mathbf{b}$ , for simplicity, we denote  $\Delta(\mathbf{z})$  as  $\Delta(\mathbf{b})$  from now on, and with  $\Phi = \mathbf{S}\Delta(\mathbf{b})$ . In line with the approach described in Fig. 1 (b), the channels  $\mathbf{t}_i$  are not known to the BS. For this reason, the optimization of the RIS requires either a direct estimation or prior knowledge of certain statistical parameters characterizing these channels. In particular, we assume  $\mathbf{t}_i \sim \mathcal{N}(\mathbf{0}, \mathbf{R}_{\mathbf{t}_i})$ , where  $\mathbf{R}_{\mathbf{t}_i}$  are the correlation matrices, with  $i = 1, \dots, N_u$ . Concerning the matrix  $\mathbf{S}$ , it is assumed to be perfectly known from the network deployment. This knowledge can be either because the BS and RIS are in fixed positions with a strong LOS component or because the BS is stationary, allowing the channel to be known through offline estimation techniques. In essence, we are considering a scenario where the RIS and the BS cannot be mounted on mobile nodes, such as UAVs or vehicles. In a scenario where the RIS and the BS can move, the problem of channel estimation becomes more complex, and the link  $\mathbf{S}$  between the BS and the RIS can also be uncertain. However, if the channel is significantly influenced by a strong LOS component, which is the only case where RIS can be beneficial as discussed above, the channel depends only on the positions. Therefore, the approach proposed in this paper remains valid, provided that sufficiently detailed information about the positions of the BS and the RIS is available. In the model considered for simulations, we will take into account the presence of a certain amount of multipath in the BS-RIS link, which results in a slight uncertainty in  $\mathbf{S}$ . We will demonstrate that this presence does not have any substantial impact.

We denote by  $\mathbf{x} = \mathbf{t}_1 s_1$ , the intended signal, and by  $\mathbf{w}_i = \mathbf{t}_i s_i$ , with  $i > 1$  the interfering users. Then we introduce:

$$\begin{aligned} \mathbf{R}_{\mathbf{x}} &= \mathbb{E}(\mathbf{x}\mathbf{x}^H) = \sigma_1^2 \mathbf{R}_{\mathbf{t}_1} \\ \mathbf{R}_{\mathbf{w}_i} &= \mathbb{E}(\mathbf{w}_i \mathbf{w}_i^H) = \sigma_i^2 \mathbf{R}_{\mathbf{t}_i} \quad i = 2, \dots, N_u. \end{aligned} \quad (8)$$

Then, emphasizing the effect of the intended UE with respect to the others, neglecting the direct links  $\mathbf{p}_i$ , we can rewrite (1) as follows:

$$\mathbf{y} = \Phi \mathbf{x} + \Phi \sum_{i=2}^{N_u} \mathbf{w}_i + \mathbf{n}. \quad (9)$$

For the purpose of optimizing the RIS, we consider the worst-case bound presented in [36] to evaluate the ergodic achievable uplink rate in the presence of interference, based on the assumption of uncorrelated additive interference and noise. Accordingly, we can write the following expression for

the ergodic uplink rate:

$$R = \mathbb{E}_{\mathbf{t}_1} [\log_2 (1 + \gamma(\mathbf{x}, \Phi, \mathbf{v}))] \quad (10)$$

where  $\mathbb{E}_{\mathbf{t}_1}$  is the expectation with respect to  $\mathbf{t}_1$  and

$$\begin{aligned} \gamma(\mathbf{x}, \Phi, \mathbf{v}) &= \frac{\sigma_1^2 \mathbf{v}^H \Phi \mathbf{t}_1 \mathbf{t}_1^H \Phi^H \mathbf{v}}{\mathbb{E}_{\mathbf{w}_i} \left( \sum_{i=2}^{N_u} \mathbf{v}^H \Phi \mathbf{w}_i \mathbf{w}_i^H \Phi^H \mathbf{v} + \mathbf{v}^H \mathbf{v} \sigma_n^2 \right)} \quad (11) \\ &= \frac{\mathbf{v}^H \Phi \mathbf{x} \mathbf{x}^H \Phi^H \mathbf{v}}{\mathbf{v}^H \left( \Phi \sum_{i=2}^{N_u} \mathbf{R}_{\mathbf{w}_i} \Phi^H + \sigma_n^2 \mathbf{I}_N \right) \mathbf{v}}. \end{aligned}$$

To elaborate from (11), we consider the upper bound  $R_b \geq R$  derived from the concavity of the logarithm function, where:

$$R_b = \log_2 \{1 + \mathbb{E}_{\mathbf{x}} [\gamma(\mathbf{x}, \Phi, \mathbf{v})]\}. \quad (12)$$

From (11) we have:

$$\mathbb{E}_{\mathbf{x}} [\gamma(\mathbf{x}, \Phi, \mathbf{v})] = \frac{\mathbf{v}^H \Phi \mathbf{R}_{\mathbf{x}} \Phi^H \mathbf{v}}{\mathbf{v}^H \left( \Phi \sum_{i=2}^{N_u} \mathbf{R}_{\mathbf{w}_i} \Phi^H + \sigma_n^2 \mathbf{I}_N \right) \mathbf{v}}. \quad (13)$$

To further elaborate, we are then in the position to formulate the optimal RIS design as:

$$\begin{aligned} (\mathbf{b}^*, \mathbf{v}^*) &= \arg \max_{\mathbf{b}, \mathbf{v}} \frac{\mathbf{v}^H \Phi(\mathbf{b}) \mathbf{R}_{\mathbf{x}} \Phi(\mathbf{b})^H \mathbf{v}}{\mathbf{v}^H \Phi(\mathbf{b}) \sum_{i=2}^{N_u} \mathbf{R}_{\mathbf{w}_i} \Phi(\mathbf{b})^H \mathbf{v} + \mathbf{v}^H \mathbf{v} \sigma_n^2} \\ &\text{s.t. } \mathbf{b} \in \mathbb{R}^M, \mathbf{v} \in \mathbb{C}^N. \end{aligned} \quad (14)$$

Regarding the variable  $\mathbf{b}$  in (14), assuming  $\mathbf{b} \in \mathbb{R}^M$ , corresponds to assuming that it is possible to implement a circuit at the ports of the RIS with any reactance value, meaning that the phases of the reflection coefficient (7) can take any value in the interval  $[0, 2\pi]$ . As for the combining vector  $\mathbf{v}^*$  resulting from the solution of problem (14) is indefinite in its magnitude, in the sense that given a  $\mathbf{v}^*$ , any  $\alpha \mathbf{v}^*$  is still optimal for all  $\alpha > 0$ . This indeterminacy will not be present in the dual problem that we will define later and which will be considered for the iterative computation of  $\mathbf{v}$ . It's worth noting that problem (14) is not convex in  $\mathbf{v}$  and  $\Phi$ , and a further difficulty arises from the complicated relationship between  $\Phi$  and  $\mathbf{b}$  entailed by MP models due to the matrix inversion in (2). Hence, we provide an alternative formulation of the same problem in the following, which allows us to find a local optimum.

The proposed approach is based on alternating optimization (AO). The AO algorithm, known for breaking down optimization tasks into smaller, more manageable subproblems, simplifies the optimization process. This approach proves particularly useful when dealing with intricate interactions or dependencies among variables. Specifically, a three-steps algorithm is proposed in which, in addition to the two variables  $\mathbf{v}$  and  $\mathbf{b}$  present in (14), there is an auxiliary variable  $\Lambda$  that will be introduced later. These variables are alternately optimized, i.e., one of the three variables is

optimized assuming the other two fixed. To start, let's consider being at iteration  $k$  of the AO algorithm, and we denote by  $\mathbf{v}^{(k)}$  and  $\mathbf{b}^{(k)}$  the values of  $\mathbf{v}$  and  $\mathbf{b}$  found at iteration  $k$ . Then, a method is derived for computing  $\mathbf{b}^{(k+1)}$  with the precoder fixed to  $\mathbf{v}^{(k)}$ , which for simplicity of notation is simply denoted as  $\mathbf{v}$ .

### B. RIS optimization

Given the precoding vector  $\mathbf{v}$ , we formulate problem (14) as follows:

$$\mathbf{b}^* = \arg \max_{\mathbf{b}} \frac{\mathbf{v}^H \Phi(\mathbf{b}) \mathbf{R}_x \Phi(\mathbf{b})^H \mathbf{v}}{\mathbf{v}^H \Phi(\mathbf{b}) \left( \sum_{i=2}^{N_u} R_{\mathbf{w}_i} \Phi(\mathbf{b})^H \mathbf{v} + \mathbf{v}^H \mathbf{v} \sigma_n^2 \right)} \quad (15)$$

s.t.  $\mathbf{b} \in \mathbb{R}^M$ .

Problem (15) remains non-convex in  $\Phi$ .

To elaborate, consider the eigen-decomposition  $\mathbf{R}_x = \mathbf{U} \mathbf{D} \mathbf{U}^H$ . Since  $\mathbf{R}_x$  is positive semidefinite, the diagonal matrix  $\mathbf{D}$  has real non-negative entries. Then, we introduce the auxiliary variable vector  $\Lambda \in \mathbb{C}^{M \times 1}$  and the error function (16). In Appendix A, we will provide an interpretation of the meaning of these terms within the context of an LMMSE estimation problem. The estimation problem can be seen as a dual problem, which, as we will see, is formally identical to the primary problem defined in (14). Therefore, the estimator  $\Lambda$  will simply represent an auxiliary variable of the original problem, allowing us to reformulate the objective function in (15) in such a way as to decompose it into two convex subproblems.

Going along with the interpretation of the dual estimation problem, the optimal estimator  $\Lambda$  from equation (16) can be defined as:

$$\begin{aligned} \Lambda^*(\Phi, \mathbf{v}) &= \arg \min_{\Lambda} \mathcal{E}_r(\Lambda, \Phi, \mathbf{v}) \\ &= \frac{\mathbf{D}^{1/2} \mathbf{U}^H \Phi^H \mathbf{v}}{\mathbf{v}^H \left( \Phi \mathbf{R}_x \Phi^H + \Phi \sum_{i=2}^{N_u} R_{\mathbf{w}_i} \Phi^H + \sigma_n^2 \mathbf{I}_N \right) \mathbf{v}}. \end{aligned} \quad (17)$$

Substituting (17) into (16) yields:

$$\mathcal{E}_r^*(\Phi, \mathbf{v}) = \text{tr} \left( \mathbf{I}_M - \Lambda^*(\Phi, \mathbf{v}) \mathbf{v}^H \Phi \mathbf{U} \mathbf{D}^{1/2} \right). \quad (18)$$

Denoting  $\mathbf{s} = \mathbf{D}^{1/2} \mathbf{U}^H \Phi^H \mathbf{v}$ , from (17), (18) can be written as:

$$\begin{aligned} \mathcal{E}_r^*(\Phi, \mathbf{v}) &= M - \frac{\mathbf{s}^H \mathbf{s}}{\mathbf{v}^H \left[ \Phi \left( \mathbf{R}_x + \sum_{i=2}^{N_u} R_{\mathbf{w}_i} \right) \Phi^H + \sigma_n^2 \mathbf{I}_N \right] \mathbf{v}} \\ &= M - 1 + \frac{1}{\mathbb{E}_x[\gamma(\mathbf{x}, \Phi, \mathbf{v})] + 1}. \end{aligned} \quad (19)$$

Thus, problem (15) is equivalent to:

$$\begin{aligned} \mathbf{b}^* &= \arg \min_{\mathbf{b}} \left[ \min_{\Lambda} \mathcal{E}_r(\Lambda, \Phi, \mathbf{v}) \right] \\ \text{s.t. } \mathbf{b} &\in \mathbb{R}^M \end{aligned} \quad (20)$$

To verify this result, it suffices to note that the minimum of  $\mathcal{E}_r$  in (20) corresponds to  $\mathcal{E}_r^*$  calculated in (19), which depends on the inverse of  $\mathbb{E}_x[\gamma(\mathbf{x}, \Phi, \mathbf{v})]$ . Therefore, minimizing this term is equivalent to maximizing  $\mathbb{E}_x[\gamma(\mathbf{x}, \Phi, \mathbf{v})]$ , which is the original problem in (15). To solve problem (20), following the AO approach, the two minimization problems are computed separately. Specifically, we proceed as follows:

- 1) With  $\Phi = \Phi(\mathbf{b}^{(k)})$ , we compute  $\Lambda^{(k+1)}$  as (17):

$$\Lambda^{(k+1)} = \Lambda^*(\Phi(\mathbf{b}^{(k)}), \mathbf{v}). \quad (21)$$

- 2) The RIS phase-shift matrix is computed as the solution of the minimization

$$\begin{aligned} \mathbf{b}^{(k+1)} &= \arg \min_{\mathbf{b}} \mathcal{E}_r(\Lambda^{(k+1)}, \Phi(\mathbf{b}), \mathbf{v}) \\ \text{s.t. } \mathbf{b} &\in \mathbb{R}^M. \end{aligned} \quad (22)$$

### C. Solution of (22)

To elaborate, for the sake of notation convenience, let us introduce  $Q$  and  $\mathbf{q} \in \mathbb{C}^{M \times 1}$  as:

$$\begin{aligned} Q &= \mathbf{v}^H \left( \Phi(\mathbf{b}) \left( \mathbf{R}_x + \sum_{i=2}^{N_u} R_{\mathbf{w}_i} \right) \Phi^H(\mathbf{b}) + \sigma_n^2 \mathbf{I}_N \right) \mathbf{v} \\ \mathbf{q} &= \mathbf{v}^H \Phi(\mathbf{b}) \mathbf{U} \mathbf{D}^{1/2}. \end{aligned} \quad (23)$$

It is then easy to show that:

$$\begin{aligned} \mathcal{E}_r(\Lambda^{(k+1)}, \Phi(\mathbf{b}), \mathbf{v}) &= \left\| \Lambda^{(k+1)} \right\|^2 Q \\ &\quad - 2\Re \sum_{j=1}^M \left[ \Lambda_j^{(k+1)} q_j \right] + M. \end{aligned} \quad (24)$$

The proposed approach to RIS optimization utilizes the Neumann series approximation to linearize the matrix inverses for small variations of the solution, similar to traditional Z-matrix-based approaches (see, e.g., [16]). However, as demonstrated in [21], working with the phase of the reflection coefficients rather than directly with the tunable reactances  $\mathbf{b}$  leads to better performance in terms of algorithm convergence. For further clarification, when neglecting the parasitic resistance  $r_0$ , the reflection coefficient  $\Gamma_m$  of the  $m$ -th port of the RIS becomes a pure phase shift, i.e.,  $\Gamma_m = e^{j\phi_m}$ , and we can

---


$$\mathcal{E}_r(\Lambda, \Phi, \mathbf{v}) = \text{tr} \left\{ \Lambda \left[ \mathbf{v}^H \left( \Phi \left( \mathbf{R}_x + \sum_{i=2}^{N_u} R_{\mathbf{w}_i} \right) \Phi^H + \sigma_n^2 \mathbf{I}_N \right) \mathbf{v} \right] \Lambda^H - 2\Re \left[ \Lambda \mathbf{v}^H \Phi \mathbf{U} \mathbf{D}^{1/2} \right] + \mathbf{I}_M \right\}. \quad (16)$$

express it as:

$$\begin{aligned} \Gamma_m &= \frac{jb_m - Z_0}{jb_m + Z_0} \rightarrow b_m = \frac{Z_0}{j} \frac{1 + e^{j\phi_m}}{1 - e^{j\phi_m}} \\ \frac{db_m}{d\phi_m} &= 2Z_0 \frac{e^{j\phi_m}}{(e^{j\phi_m} - 1)^2} = \\ &= 2Z_0 \frac{jb_m - Z_0}{(jb_m + Z_0) \left( \frac{jb_m - Z_0}{jb_m + Z_0} - 1 \right)^2} = -\frac{b_m^2 + Z_0^2}{2Z_0}. \end{aligned} \quad (25)$$

Hence, denoting by  $\mathbf{B}^{(k)} = \text{diag}(\mathbf{b}^{(k)})$  and  $\phi^{(k)}$  the tunable reactances matrices and the corresponding reflection coefficient phase vector at iteration  $k$  of the iterative algorithm and considering small variations of  $\phi^{(k)}$  for evaluating the solution at next step, i.e.,  $\phi^{(k+1)} = \phi^{(k)} + \delta$ , with  $\delta \in \mathbb{C}^{1 \times M}$  and  $\delta_m \ll 1$ , we have:

$$\mathbf{B}^{(k+1)} \approx \mathbf{B}^{(k)} + \mathbf{F}^{(k)} \text{diag}(\delta) \quad (26)$$

where  $\mathbf{F}^{(k)} \in \mathbb{C}^{M \times M}$  is a diagonal matrix with entries  $\mathbf{F}_{m,m}^{(k)} = -\frac{(b_m^{(k)})^2 + Z_0^2}{2Z_0}$ .

1) *Solution for the MP model:* Since  $\Phi = \mathbf{S}\Delta(\mathbf{b})$ , from (2) and (23) we have:

$$Q = 4Y_0^2 \mathbf{v}^H \left\{ \mathbf{S}(\mathbf{Z}_{SS} + r_0 + j\mathbf{B})^{-1} \left( \mathbf{R}_x + \sum_{i=2}^{N_u} R_{\mathbf{w}_i} \right) \right. \quad (27)$$

$$\left. \times [\mathbf{S}(\mathbf{Z}_{SS} + r_0 + j\mathbf{B})^{-1}]^H + \sigma_n^2 \mathbf{I}_N \right\} \mathbf{v}$$

$$\mathbf{q} = -2Y_0 \mathbf{v}^H \mathbf{S}(\mathbf{Z}_{SS} + r_0 + j\mathbf{B})^{-1} \mathbf{U} \mathbf{D}^{1/2}.$$

From (26) we have:

$$\begin{aligned} \mathbf{S}(\mathbf{Z}_{SS} + r_0 + j\mathbf{B}^{(k+1)})^{-1} \\ \approx \mathbf{S}(\mathbf{Z}_{SS} + r_0 + j\mathbf{B}^{(k)} + j\mathbf{F}^{(k)} \text{diag}(\delta))^{-1}. \end{aligned} \quad (28)$$

We then introduce the following terms:

$$\begin{aligned} \mathbf{A}^{(k)} &= (\mathbf{Z}_{SS} + r_0 + j\mathbf{B}^{(k)})^{-1} \\ \mathbf{G}^{(k)} &= j\mathbf{S}\mathbf{A}^{(k)}\mathbf{F}^{(k)}. \end{aligned} \quad (29)$$

Invoking the Neumann series approximation for matrix inversion, we have:

$$\mathbf{S}(\mathbf{Z}_{SS} + r_0 + j\mathbf{B}^{(k+1)})^{-1} \approx \mathbf{S}\mathbf{A}^{(k)} - \mathbf{G}^{(k)} \text{diag}(\delta) \mathbf{A}^{(k)} \quad (30)$$

where the approximation holds when:

$$\left\| \mathbf{F}^{(k)} \text{diag}(\delta) (\mathbf{Z}_{SS} + r_0 + j\mathbf{B}^{(k)})^{-1} \right\| \leq \epsilon \quad (31)$$

with  $\epsilon \ll 1$ . Denoting by  $\mathbf{P} = \mathbf{F}^{(k)}\mathbf{A}^{(k)}$ , condition (31) can be expressed as:

$$\sum_{m=1}^M \delta_m^2 \theta_m^2 < \epsilon^2 \quad (32)$$

where  $\theta_m$  represents the entries of the main diagonal of  $\mathbf{P}\mathbf{P}^H$ . Then:

$$\begin{aligned} Q &\approx 4Y_0^2 \mathbf{v}^H \left\{ (\mathbf{S}\mathbf{A}^{(k)} - \mathbf{G}^{(k)} \text{diag}(\delta) \mathbf{A}^{(k)}) \left( \mathbf{R}_x + \sum_{i=2}^{N_u} R_{\mathbf{w}_i} \right) \right. \\ &\quad \times [\mathbf{S}\mathbf{A}^{(k)} - \mathbf{G}^{(k)} \text{diag}(\delta) \mathbf{A}^{(k)}]^H + \sigma_n^2 \mathbf{I}_N \left. \right\} \mathbf{v} \\ \mathbf{q} &\approx -2Y_0 \mathbf{v}^H (\mathbf{S}\mathbf{A}^{(k)} - \mathbf{G}^{(k)} \text{diag}(\delta) \mathbf{A}^{(k)}) \mathbf{U} \mathbf{D}^{1/2}. \end{aligned} \quad (33)$$

From (24) and (33), problem (22) is then a convex problem in  $\delta$  with solution  $\delta^*$  that can be evaluated as shown in Appendix B. Finally, we can evaluate

$$\begin{aligned} \mathbf{B}^{(k+1)} &= \mathbf{B}^{(k)} + \mathbf{F}^{(k)} \text{diag}(\delta^*) \\ \mathbf{b}^{(k+1)} &= \text{diag}(\mathbf{B}^{(k+1)}) \end{aligned} \quad (34)$$

and go to the next iteration of the AO algorithm.

2) *Solution for the CT model:* In the CT case, it is necessary to use (4) instead of (2). This firstly entails using a diagonal  $\mathbf{Z}_{SS}$  with entries  $Z_0$ , which is trivial and does not lead to differences regarding the solution of problem (22). Secondly, it is necessary to subtract  $\Delta_S$  in (30), resulting in:

$$\begin{aligned} \mathbf{S}(\mathbf{Z}_{SS} + r_0 + j\mathbf{B}^{(k+1)})^{-1} \\ \approx \mathbf{S}\mathbf{A}^{(k)} - \mathbf{G}^{(k)} \text{diag}(\delta) \mathbf{A}^{(k)} - \Delta_S. \end{aligned} \quad (35)$$

From this point onwards, the optimization can proceed straightforwardly in the same manner as described above for the MP case.

#### D. Combiner optimization

For the computation of the combiner  $\mathbf{v}^{(k+1)}$ , another step of AO is performed. Specifically, with the RIS tunable vector fixed to  $\mathbf{b}^{(k+1)}$ , which for simplicity of notation is denoted as  $\mathbf{b}$ , we have:

$$\mathbf{v}^{(k+1)} = \arg \min_{\mathbf{v}} \mathcal{E}_{\mathbf{r}}(\mathbf{A}^{(k+1)}, \Phi(\mathbf{b}), \mathbf{v}). \quad (36)$$

Note that the computation of  $\mathbf{v}$  in (36) is not indeterminate in magnitude, as it is effectively a vector that minimizes a mean squared error. From (24) and (23), introducing

$$\mathbf{W} = \Phi(\mathbf{b}) \left( \mathbf{R}_x + \sum_{i=2}^{N_u} R_{\mathbf{w}_i} \right) \Phi^H(\mathbf{b}) + \sigma_n^2 \mathbf{I}_N \quad (37)$$

we get:

$$\begin{aligned} \mathcal{E}_{\mathbf{r}}(\mathbf{A}^{(k+1)}, \Phi(\mathbf{b}), \mathbf{v}) &= \mathbf{v}^H \left\| \mathbf{A}^{(k+1)} \right\|^2 \mathbf{W} \mathbf{v} \\ &\quad - 2\Re \left( \mathbf{A}^{(k+1)} \mathbf{v}^H \Phi(\mathbf{b}) \mathbf{U} \mathbf{D}^{1/2} \right) + r. \end{aligned} \quad (38)$$

The problem in (36) is convex and can be solved by setting the gradient to zero. To elaborate, we can evaluate the gradient as:

$$\begin{aligned} \nabla_{\mathbf{v}} \left[ \mathcal{E}_{\mathbf{r}}(\mathbf{A}^{(k+1)}, \Phi(\mathbf{b}), \mathbf{v}) \right] \\ = 2 \left\| \mathbf{A}^{(k+1)} \right\|^2 \mathbf{W} \mathbf{v} - 2\Phi(\mathbf{b}) \mathbf{U} \mathbf{D}^{1/2} \mathbf{A}^{(k+1)}. \end{aligned} \quad (39)$$

---

**Algorithm 1:** Proposed Optimization Algorithm
 

---

**Input:**  $\mathbf{S}, \mathbf{R}_{t_i}, i = 1, \dots, N_u, \sigma_n^2, \mathbf{Z}_{SS}, Z_0 = 50 \Omega, r_0 > 0$ ;  
**Initialize:**  
 Generate the initial values of  $\mathbf{v}^{(0)}$  and  $\mathbf{b}^{(0)}$  and evaluate  $\Phi^{(0)} = \mathbf{S}\Delta(\mathbf{b}^{(0)})$  and  $\Lambda^{(1)}$  according to (17);  
 Set an arbitrarily small value  $\eta > 0, \rho > \eta, k \leftarrow 0$ ;  
**while**  $\rho > \eta$  **do**  
   Compute  $\mathbf{b}^{(k+1)}$  according to (34);  
   Compute  $\mathbf{v}^{(k+1)}$  according to (40);  
   Compute  $\Lambda^{(k+2)}$  according to (17);  
    $\rho \leftarrow \|\mathbf{b}^{(k+1)} - \mathbf{b}^{(k)}\|$ ;  
    $k \leftarrow k + 1$ .  
**end while**

---

Accordingly, we obtain:

$$\mathbf{v}^{(k+1)} = \left[ \left\| \Lambda^{(k+1)} \right\|^2 \mathbf{W} \right]^{-1} \Phi(\mathbf{b}) \mathbf{U} \mathbf{D}^{1/2} \Lambda^{(k+1)}. \quad (40)$$

The complete algorithm for the proposed is summarized in Algorithm 1.

#### E. Convergence of Algorithm 1

The AO approach guarantees that at each iteration:

$$\begin{aligned} \mathcal{E}_{\mathbf{r}} \left( \Lambda^{(k+2)}, \mathbf{b}^{(k+1)}, \mathbf{v}^{(k+1)} \right) &\stackrel{(a)}{\leq} \mathcal{E}_{\mathbf{r}} \left( \Lambda^{(k+1)}, \mathbf{b}^{(k+1)}, \mathbf{v}^{(k+1)} \right) \\ &\stackrel{(b)}{\leq} \mathcal{E}_{\mathbf{r}} \left( \Lambda^{(k+1)}, \mathbf{b}^{(k+1)}, \mathbf{v}^{(k)} \right) \stackrel{(c)}{\leq} \mathcal{E}_{\mathbf{r}} \left( \Lambda^{(k+1)}, \mathbf{b}^{(k)}, \mathbf{v}^{(k)} \right) \end{aligned} \quad (41)$$

where (a) follows from  $\Lambda^{(k+2)} = \Lambda^* \left( \Phi(\mathbf{b}^{(k+1)}), \mathbf{v}^{(k+1)} \right)$  (21), (b), and (c) follow from (36) and (22), respectively. From (41) and (19), we have then:

$$\mathbb{E}_{\mathbf{x}} \left[ \gamma \left( \mathbf{x}, \Phi^{(k+1)}, \mathbf{v}^{(k+1)} \right) \right] \geq \mathbb{E}_{\mathbf{x}} \left[ \gamma \left( \mathbf{x}, \Phi^{(k)}, \mathbf{v}^{(k)} \right) \right], \quad (42)$$

i.e., the objective function in (14) increases at each iteration which guarantees the convergence of Algorithm 1.

#### F. Computational Complexity

The computational complexity of Algorithm 1 depends on the complexity of evaluating the terms  $\mathbf{b}^{(k+1)}$ ,  $\mathbf{v}^{(k+1)}$ , and  $\Lambda^{(k+2)}$ , as well as on the number of iterations required to achieve convergence, which is analyzed in the Results Section. Regarding the complexity of evaluating the terms in the main body of Algorithm 1, we assume that the number of elements in the RIS is significantly greater than the number of antennas at the BS, i.e.,  $M \gg N$ . Moving forward, we adopt the customary assumption that the computational cost of computing the inverse of a matrix depends on the cube of the number of its elements. Additionally, for simplicity, we assume that the product of an  $n \times p$  matrix by a  $p \times q$  matrix entails a number of operations proportional to  $npq$ , neglecting the potential optimization from specialized algorithms for matrix multiplication.

Accordingly, it can be demonstrated that the complexity of evaluating  $\mathbf{v}^{(k+1)}$  is  $\mathcal{O}(NM^2)$  due to the evaluation of  $\mathbf{W}$  in (52). Similarly, the computation of  $\Lambda^{(k+2)}$  also incurs a complexity of  $\mathcal{O}(NM^2)$  due to the evaluation of the denominator in (17). Finally, the evaluation of  $\mathbf{b}^{(k+1)}$  has

a complexity of  $\mathcal{O}(M^3)$ , stemming from the evaluation of  $\Lambda^{(k)}$  in (29) and the matrix inversion in (56). Therefore, considering only the most significant terms, the complexity of each iteration of Algorithm 1 is  $\mathcal{O}(M^3)$ . Thus, the total complexity turns out to be  $\mathcal{O}(N_{\text{it}}M^3)$ , with  $N_{\text{it}}$  being the number of iterations of the algorithm. Despite this number potentially being high, as shown in Fig. 5, it should be noted that the proposed statistical CSI scenario allows for a considerable relaxation of complexity constraints. This is because RIS optimization can be performed over relatively long timescales on the order of seconds or even longer, depending on the user's mobility. Given the computing power of modern multi-GPU tera-flops processors, it can reasonably be assumed that the proposed algorithm is compatible with real-time implementation, particularly for low-mobility users. In calculating the complexity, it should be considered that we evaluate the complexity of a single RIS serving one node, which is the scenario of interest. If we wanted the same RIS to serve multiple nodes, or multiple RISs located in different places to serve multiple nodes, the complexity would obviously increase with the number of nodes. The analysis of this scenario is beyond the scope of the present work and could be the subject of further study.

#### V. NUMERICAL RESULTS

We present some numerical results to assess the effectiveness of the proposed optimization algorithms. Considering the scenario depicted in Fig. 2, we assume the carrier frequency is  $f_0 = 30$  GHz, the RIS is centered at position  $P_R = (0, 0, 3)$  m, and the BS is positioned at  $P_{BS} = (-7, 7, 2)$  m, corresponding to an angle of  $-\pi/4$  with respect to the RIS. The  $N_u$  UEs are situated at positions  $P_i = (X_i, Y_i, 0)$  m, with  $X_i, Y_i \geq 0$  indicating that they are located on the opposite side of the room from the BS. Specifically,  $P_0$  is the position of the user of interest and  $P_i, i > 0$  are the positions of the interfering users.

Following the RIS structure proposed in [21], the scatterers of the RIS consist of identical metallic dipoles with a radius of  $\lambda/500$  and a length of  $L = 0.46\lambda$ . The dipoles are configured as a uniform planar array (UPA) with  $M_H$  elements along the  $x$  axis and  $M_V$  elements along the  $z$  axis. The spacing between the elements is set to  $d_x = \lambda/Q$  in the  $x$  direction, where  $Q$  is an integer determining the dipole density. Conversely, the spacing between elements in the  $z$  direction is  $d_z = 3/4\lambda$ . We then choose  $M_H = 16\lambda/d_x$  and  $M_V = 4$ , resulting in an RIS forming a rectangle with an area of  $50\lambda^2$ . Regarding the BS, it is equipped with  $N = 16$  antennas arranged in two linear arrays along the  $z$  axis, with each array containing 8 antennas along the  $x$  axis. The antennas at the BS are separated by  $\lambda/2$  in the  $x$ -axis and  $3\lambda/4$  in the  $z$ -axis. Similar to the RIS, these antennas are metallic dipoles with a radius of  $\lambda/500$  and a length of  $L = 0.46\lambda$ . Regarding the noise, the variance  $\sigma^2$  is calculated to achieve a signal-to-noise ratio of -20 dB in the case where the RIS is configured randomly and for a transmitted power  $P_{tx} = 20$  dBm. Then, the UEs are equipped with single dipole antennas having the same characteristics. Finally, regarding the value



of  $\epsilon$  defined in (31), it is set equal to 0.005 which has been experimentally shown to guarantee always convergence of the iterative algorithm.

In the next two sections, we describe how the channel models for RIS optimization and simulations are generated. The two models are generated independently to reflect the fact that, in a scenario like the one considered, the RIS is optimized using a priori information that can reasonably be assumed to be known but does not perfectly reflect the real situation, i.e., there can be a mismatch.

#### A. Model considered for RIS optimization

Given the potential presence of both Line of Sight (LOS) and non-Line of Sight (NLOS) components in practical channels, we characterize the RIS-UE channel using a generalized spatially correlated Rician fading model [37]. This approach is widely used in the literature to account for the presence of multipath fading in RIS-aided communications, as shown, for example, in [38] for a MP network model using S-parameters. As for the LOS scenario, it is assumed that the prior positions of the nodes are known with circular uncertainty, meaning that the nodes are uniformly distributed within a circle of radius  $\sigma$  around the actual position, where  $\sigma$  represents the localization error. The correlation matrices of the LOS components are then computed using a classical model for correlation calculation based on the angular spread with which the signal can arrive given the known localization error. For simplicity, consider a planar geometry where the arrival angle depends only on the angle of arrival (AOA)  $\varphi$ , and assume knowledge of the range  $\Delta_i$  of possible arrival angles for the signal from  $i$ -th UE, given its uncertainty region (see the illustrative example in Fig. 3). Denoting by  $x_m$  the  $x$  location of the  $m$ -th dipole of the RIS, with  $m = 1, \dots, M$ , when a plane-wave impinges on the RIS from the AOA  $\varphi$ , the array response vector can be written as [39]

$$\mathbf{a}(\varphi) = \left[ e^{j \frac{2\pi}{\lambda} x_1 \sin \varphi}, \dots, e^{j \frac{2\pi}{\lambda} x_M \sin \varphi} \right]^T \quad (43)$$

where  $\lambda$  is the wavelength. Hence, the channel correlation matrices  $\mathbf{R}_i$  are evaluated as:

$$\mathbf{R}_i = \frac{K_1}{K_1 + 1} \beta_i \int_{\varphi_i - \Delta_i/2}^{\varphi_i + \Delta_i/2} f(\varphi, \Delta_i) \mathbf{a}(\varphi) \mathbf{a}^H(\varphi) d\varphi \quad (44)$$

where  $K_1$  is the Ricean factor,  $f(\varphi_i, \Delta_i)$  is the spatial scattering distribution function, which is derived from the uniform distribution assumption within the circle and is evaluated numerically,  $\beta_i$  represents the channel gain considering the center of the nodes' uncertainty region, which is evaluated assuming a line-of-sight (LOS) propagation model. It is important to note that this model is equivalent to the spatial correlation matrix model proposed in [39], [40]. However, in this case, this model is considered only for RIS optimization purposes and does not reflect the model generated in the simulations, as explained below. The same model is assumed for the non-line-of-sight (NLOS) component. Specifically, considering a uniform angular distribution and an angular spread  $\Delta_m$ , the correlation matrix of the NLOS part is given

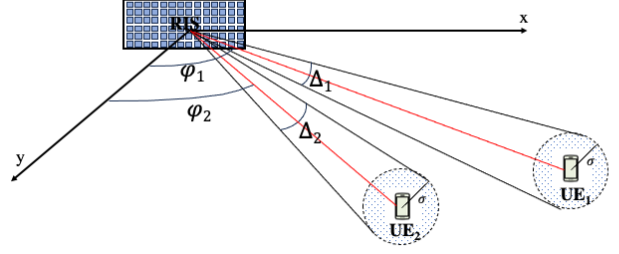


Fig. 3: Angle spread for correlation evaluation

by:

$$\mathbf{W}_i = \frac{\beta_i}{K_1 + 1} \int_{\varphi_i - \Delta_m/2}^{\varphi_i + \Delta_m/2} \mathbf{a}(\varphi) \mathbf{a}^H(\varphi) d\varphi. \quad (45)$$

Hence, making the reasonable assumption that the LOS and NLOS components are uncorrelated, we evaluate  $\mathbf{R}_x = \mathbf{R}_1 + \mathbf{W}_1$  and  $\mathbf{R}_w = \mathbf{R}_i + \mathbf{W}_i$ , with  $i > 1$ <sup>1</sup>.

To summarize, the only information known a priori for RIS optimization are:

- The uncertainty in the positions of the nodes;
- The Ricean factor;
- The angular spread of the multipath components.

#### B. Model considered for Simulations

Given the estimated positions of the nodes, the true positions are generated according to the uncertainty model, which selects a random point within the circle of the uncertainty region. Note that, as demonstrated in [31], the assumption of Gaussian correlation of the channels previously made holds reasonably well when the channel uncertainty is due to uncertainty in the node's position, although there may be a certain degree of mismatch with the model. Meanwhile, the BS is positioned at a fixed location. Subsequently, the Line of Sight (LOS) components of the matrices  $\mathbf{S}$  and the vectors  $\mathbf{t}_i$ , along with the matrix  $\mathbf{Z}_{SS}$ , are derived from the MP network model introduced in [15], utilizing the nodes' positions. This model's accuracy has been confirmed in [21] through comparison with a full-wave numerical simulator. Subsequently, following the Ricean channel model outlined earlier, a Gaussian NLOS component is incorporated. Specifically, if  $\mathbf{S}$  and  $\mathbf{t}_i$  represent the terms computed by the model [15], the actual  $\mathbf{S}^{(e)}$  and  $\mathbf{t}_i^{(e)}$  are determined by introducing multipath effects in the form of additive Gaussian noise with a covariance matrix calculated as in (45). Notably, we generate the NLOS for the  $i$ -th RIS-UE channels, taking into account the angle spreading  $\Delta_m$  and the Ricean factor  $K_1$ . For the BS-RIS channel, we consider the angle spreading  $\Delta_m^{(BS)}$  and a Ricean factor  $K_0$ . It's worth mentioning that although we include the NLOS component in the BS-RIS channel in the simulations, this effect is not

<sup>1</sup>NLOS depends on the presence of natural scatterers in the environment, which introduce attenuation and phase shifts entirely different from those of LOS (Line-of-Sight).

accounted for in the analysis, assuming that  $K_0$  can be very high. Regarding the direct path BS-UE, it is assumed that only an NLOS component may be present with power lower than that reflected by the RIS, which is the situation of interest for RIS-aided communications. In particular, to stay general, it is assumed that the direct path BS-UE is modeled through an NLOS multipath channel generated according to a Rayleigh distribution with a power  $K_{DP}$  times lower than the signal received from the RIS. The direct channels between the BS and the  $i$ th UE are denoted by  $\mathbf{p}_i^{(e)} \in \mathbb{C}^{N \times 1}$ .

### C. Performance evaluation

During actual transmission, the RIS becomes an integral part of the environment, and communication follows standard end-to-end channel estimation strategies, which can be conducted with pilot sequences and receiver CSI estimation. Specifically, the end-to-end channels are  $\mathbf{h}_i^{(e)} = \mathbf{p}_i^{(e)} + \Phi^{(e)} \mathbf{t}_i^{(e)}$  where  $\Phi^{(e)} = \mathbf{S}^{(e)} \Delta(\mathbf{b})$  depends on the RIS configuration  $\mathbf{b}$  optimized offline. Accordingly, the rate for each channel instance is computed as:

$$R_e = \log_2 \left( 1 + \frac{\sigma_1^2 \mathbf{v}^H \mathbf{h}_1^{(e)} (\mathbf{h}_1^{(e)})^H \mathbf{v}}{\sum_{i=2}^{N_u} \sigma_i^2 \mathbf{v}^H \mathbf{h}_i^{(e)} (\mathbf{h}_i^{(e)})^H \mathbf{v} + \mathbf{v}^H \mathbf{v} \sigma_n^2} \right) \quad (46)$$

where the combining vector  $\mathbf{v}$  is evaluated according to the MMSE criterion, which is known to optimize Shannon capacity.

### D. Results

In the following figures, we present the results obtained from simulations to validate the optimization approach proposed in Section IV. The results are obtained for three different schemes, namely:

- OPT-NoCSI - Optimal RIS design with MP model for RIS and statistical CSI;
- CT-CSI - Optimal RIS design with CT model for RIS and statistical CSI;
- OPT-CSI - Optimal RIS design with MP model and instantaneous CSI;

In all cases, the results are calculated by averaging the effective rate computation reported in (46) over a certain number of channel instances generated according to the procedure described in Section V-B. Regarding the OPT-CSI case, it refers to the scenario in which the RIS is optimized based on the exact knowledge of the channel of the intended user. To this aim, in place of the ergodic rate defined in (10), we refer to the instantaneous uplink rate:

$$R = \log_2 \left( 1 + \gamma(\mathbf{t}_1^{(e)}, \Phi, \mathbf{v}) \right) \quad (47)$$

where

$$\gamma(\mathbf{t}_1^{(e)}, \Phi, \mathbf{v}) = \frac{\sigma_1^2 \mathbf{v}^H \Phi \mathbf{t}_1^{(e)} (\mathbf{t}_1^{(e)})^H \Phi^H \mathbf{v}}{\mathbf{v}^H \left( \Phi \sum_{i=2}^{N_u} R_{\mathbf{w}_i} \Phi^H + \sigma_n^2 \mathbf{I}_N \right) \mathbf{v}}.$$

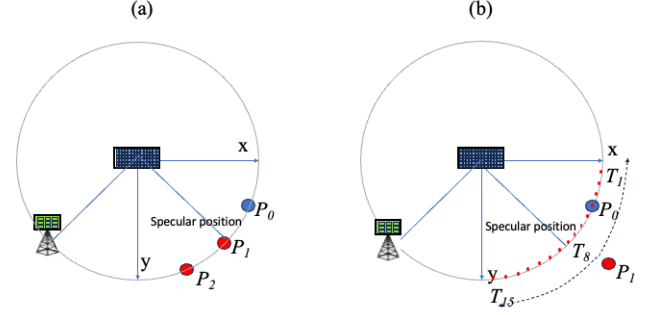


Fig. 4: Simulation scenarios: (a) Scenario adopted for the results in fig. 5; (b) Scenario adopted for the results in figs. 6-9.

Hence, the optimization problem can be written as in (14) considering  $\mathbf{R}_x = \sigma_1^2 \mathbf{t}_1^{(e)} (\mathbf{t}_1^{(e)})^H$ . With this modification, Algorithm 1 allows for maximizing the instantaneous rate instead of the average rate. OPT-CSI thus provides a performance benchmark that could be achieved in the case of ideal CSI between the intended node and the RIS. Finally, in all cases the angular spread  $\Delta_m$  of the multipath components is set to  $10^\circ$  for the RIS-UE links and  $5^\circ$  for the RIS-BS link.

In Fig. 5, the convergence behavior for the OPT-NoCSI algorithm is depicted for the case illustrated in Fig. 4 (a), where  $N_u = 3$ , with positions  $P_0 = (10 \cos \pi/8, 10 \sin \pi/8, 0)$ ,  $P_1 = (10 \cos \pi/4, 10 \sin \pi/4, 0)$ , and  $P_2 = (10 \cos 3\pi/8, 10 \sin 3\pi/8, 0)$ , and for three values of dipoles' distances:  $d_x = \lambda/2$ ,  $d_x = \lambda/4$ , and  $d_x = \lambda/8$ . Specifically, the rate value (12) expressed in bit/s/Hz is plotted against the iteration index  $k$ . In other words, the node positions are assumed such that the two interfering nodes are located at the same distance of 10 meters from the useful node, corresponding to the case where the signal-to-interference ratio (SIR) is equal to 1, with angles between the nodes differing by  $\pi/8$ . Note that assuming that all nodes are at the same distance serves to consider a scenario of consistent but non-degenerate interference. It is also worth noting that, with the parameters considered, the propagation conditions correspond to the far-field case. The Ricean factors  $K_0$  and  $K_1$  for the BS-RIS and RIS-UEs links are set to  $K_0 = 20$  and  $K_1 = 10$ , respectively. Figure 5 (a), (b), (c) and (d) report the results for four different position uncertainty:  $\sigma = 0$  m,  $\sigma = 0.1$  m,  $\sigma = 0.5$  m and  $\sigma = 1$  m, respectively.

It can be observed that the proposed algorithm allows for an increasing rate  $R_b$  with iterations, thus enabling convergence to a local optimum in all cases. In this regard, it is noted that when the dipoles are spaced by  $\lambda/2$ , convergence is faster, which can be explained by the lesser effect of the non-diagonals of the  $\mathbf{Z}$  matrix. However, it is observed that the improvement in going from  $\lambda/4$  to  $\lambda/8$  is negligible at the expense of a further increase in the number of iterations needed for convergence. It is noted that this improvement is achieved for the same RIS aperture of  $50\lambda^2$ . Finally, it is observed that increasing position uncertainty results in only a slightly perceptible performance degradation. For example,

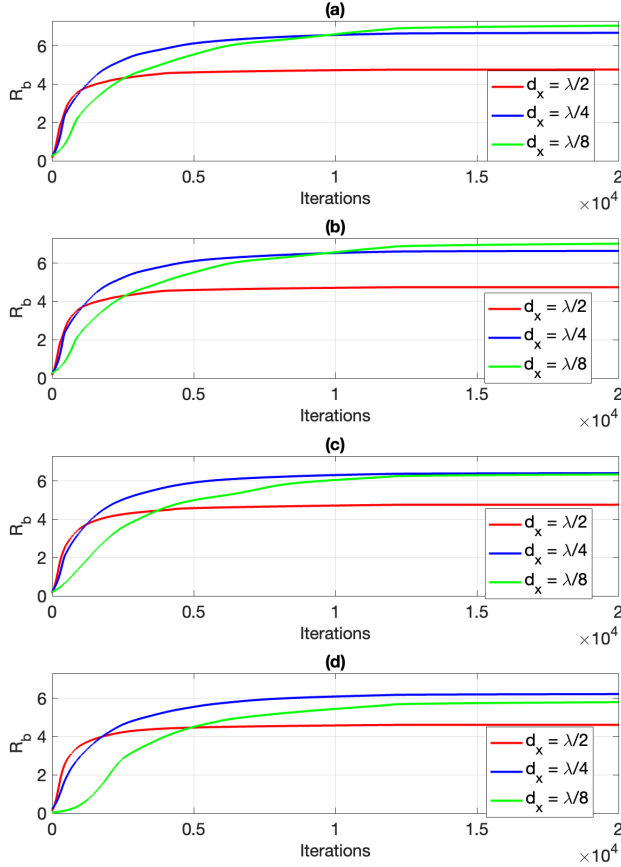


Fig. 5: Convergence behavior for the OPT-NoCSI algorithm for the case where  $N_u = 3$  and for three values of dipoles' distances:  $d_x = \lambda/2$ ,  $d_x = \lambda/4$ , and  $d_x = \lambda/8$ . The node positions are assumed such that the two interfering nodes are located at the same distance of 10 meters from the useful node, with angles between the nodes differing by  $\pi/8$ . The results for four different position uncertainty, namely  $\sigma = 0$  m,  $\sigma = 0.1$  m,  $\sigma = 0.5$  m and  $\sigma = 1$  m, are reported in Figs. (a), (b), (c) and (d), respectively.

in the case of  $\lambda/8$ , the rate decreases from approximately 6.5 to 6. It should be emphasized that this is not the actual rate measured by the simulations and reported in the subsequent graphs, but only the rate used in the objective function to optimize the RIS in the offline phase.

In Figs. 6-8, the rate  $R_e$  in (46) evaluated through several simulations is reported for  $K_{DP} = \infty$  (i.e., the direct link is not generated),  $N_u = 2$  for the case illustrated in Fig. 4 (b) with the intended UE positioned at  $P_0 = (10 \cos \pi/8, 10 \sin \pi/8, 0)$  while the interfering UE is positioned at 15 different possible positions  $P_1 = T_i = [10 \cos(i \times \pi/32), 10 \sin(i \times \pi/32)]$  with  $i = 1, 2, \dots, 15$ . Accordingly, the interfering user is at the same distance from the RIS as the useful user but with different angles. In Figs. 6-8(a), the case  $d_x = \lambda/2$  is considered, whereas in 6-8(b)  $d_x = \lambda/4$  is reported. Furthermore, the three figures 6, 7, and 8 refer to the values of  $\sigma = 0.1, 0.5, 1$  m, respectively. The curves correspond to the OPT-NoCSI, OPT-CT, and OPT-CSI cases described earlier. It is noted that at position  $T_4$ , the interfering user is on average in the same position as the intended UE, thus an average rate equal to one is expected

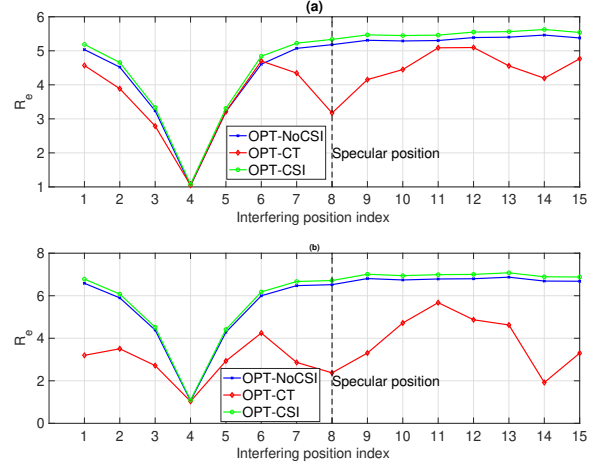


Fig. 6: Rate  $R$  in (10) evaluated through simulations without direct link in the case of  $N_u = 2$ , with the intended UE positioned at  $P_0 = 10 (\cos \pi/8, \sin \pi/8, 0)$  while the interfering user is positioned at 12 possible different positions,  $P_i = 10 \{\cos[\pi/8 + (i-1)\pi/32], \sin[\pi/8 + (i-1)\pi/32], 0\}$ , with  $i = 1, \dots, 12$ . The case (a) refers to  $d_x = \lambda/2$ , while the case (b) reports the case  $d_x = \lambda/4$ .

since  $\text{SIR} = 1$  and the interference cannot be removed, as indeed happens in all considered cases. It is also noted that at position  $T_8$ , the interfering user is at an angle  $\pi/4$ , corresponding to the specular position of the RIS with respect to the BS. In this case, it is evident that the CT model fails, as the RIS is optimized without considering the specular component, which in this case produces strong interference. In Fig. 9, the results obtained are for the same setting as in Fig. 7, except that in this case  $K_{DP} = 4$ , i.e., we include a direct link that is 6 dB weaker than the path reflected from the RIS. Note that our RIS optimization algorithm is based on the assumption that the direct path is not present. Thus, the OPT-CSI case refers to this scenario, meaning it assumes exact knowledge of the channel  $\mathbf{t}_1^{(e)}$  but not of the direct path. Nonetheless, the performance generally improves due to the presence of the direct path for both the OPT-NoCSI and OPT-CSI cases. This improvement is especially notable at position  $T_4$  when the interferer is located in the same position as the reference node. In this case, the interference from the direct path can be spatially filtered out thanks to the full-rank model chosen for the direct path channel. It is noted that the optimizer OPT-NoCSI, in many cases, manages to achieve performance reasonably close to the OPT-CSI case. This is observed in scenarios where the uncertainty in the node position is small, e.g., 0.1 m and 0.5 m. In cases where the uncertainty in the node positions is increased to 1 m, the distance between the two cases obviously increases, as expected. In any case, the performance of the OPT-noCSI case is encouraging considering the significant reduction of RIS configuration overhead.

In the last two figures, namely Figs. 10 and 11, we present the scenario where there is only one transmitting

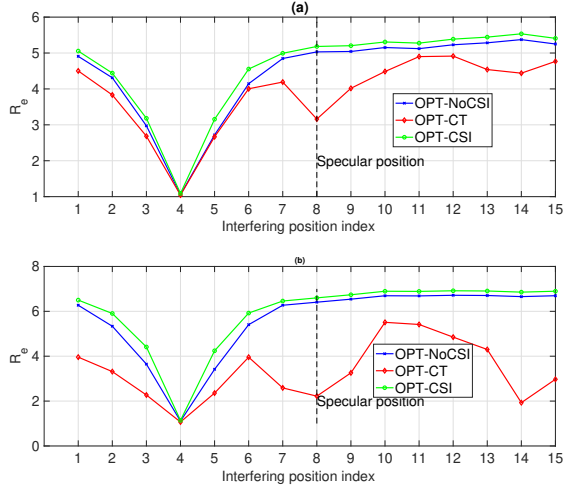


Fig. 7: Rate  $R$  in (10) evaluated through simulations considering  $\sigma = 0.5$  m for the same setting of Fig. 6.

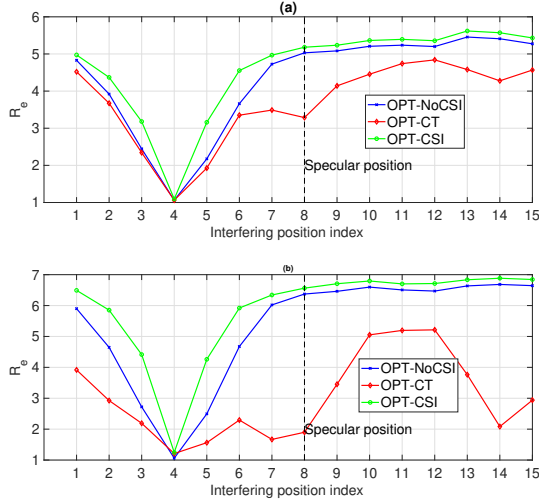


Fig. 8: Rate  $R$  in (10) evaluated through simulations considering  $\sigma = 1$  m for the same setting of Fig. 6.

node positioned at a distance of 10 m and at all possible angular positions  $\phi$  from 0 to 90 degrees. In this setting, we depict the power received at the BS (in dBW) in the absence of direct link as a function of the angle  $\phi$ . The RIS is optimized using the OPT-NoCSI and CT approaches for the case  $N_u = 2$ , where the central position of the reference node is  $P_0 = (10 \cos \frac{\pi}{8}, 10 \sin \frac{\pi}{8}, 0)$ , corresponding to an angle of 22.5 degrees, and that of the interfering node is  $P_1 = (10 \cos \frac{\pi}{4}, 10 \sin \frac{\pi}{4}, 0)$ , corresponding to the specular position at 45 degrees. In 10 (a), (b), (c), the cases  $d_x = \lambda/2$  and  $\sigma = 0.5, 1, 2$  m are depicted, respectively. In 11 (a), (b), (c), the same cases are illustrated for  $d_x = \lambda/4$ . The objective of these figures is to showcase the type of beam created by the RIS in the direction of the useful node and its ability to reject interference. Note how the OPT-NoCSI case takes into account the presence of the interfering node

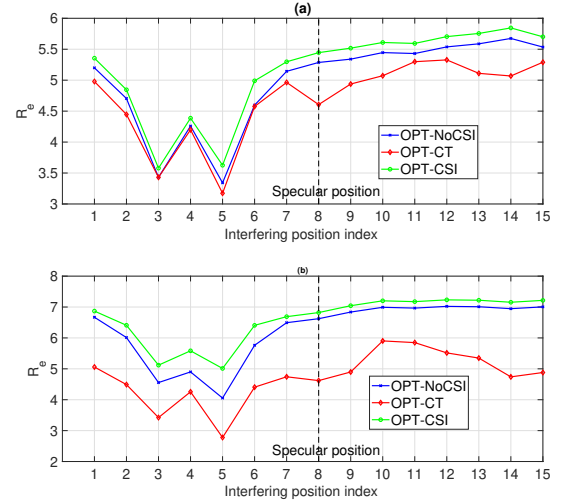


Fig. 9: Rate  $R$  in (10) evaluated through simulations with direct link characterized by  $K_{DP} = 4$ , in the case of  $N_u = 2$ , with the intended UE positioned at  $P_0 = 10 (\cos \frac{\pi}{8}, \sin \frac{\pi}{8}, 0)$  while the interfering user is positioned at 12 possible different positions,  $P_i = 10 \{\cos[\pi/8 + (i-1)\pi/32], \sin[\pi/8 + (i-1)\pi/32], 0\}$ , with  $i = 1, \dots, 12$ . The case (a) refers to  $d_x = \frac{\lambda}{2}$ , while the case (b) reports the case  $d_x = \frac{\lambda}{4}$ .

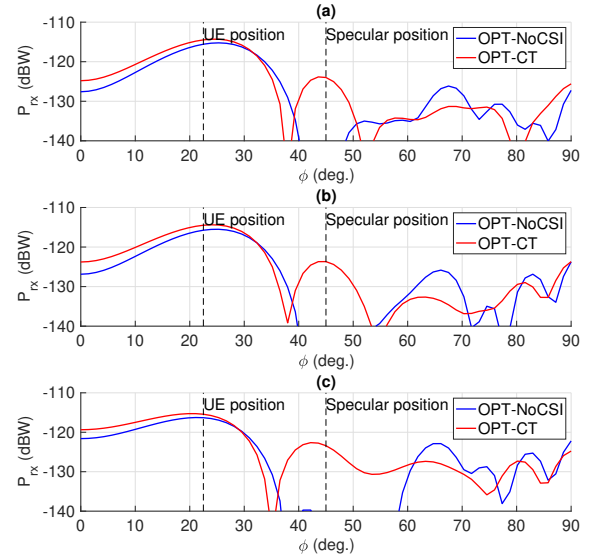


Fig. 10: Power received at the BS (in dBW) as a function of the angle  $\phi$  of the transmitting node. The RIS characterized by  $d_x = \lambda/2$  and it is optimized using the OPT-NoCSI and CT approaches for the case  $N_u = 2$ , where the reference node at an angle of 22.5 degrees, and the interfering node is at 45 degrees (specular direction).

in the specular component and creates a strong attenuation in that direction, thus significantly attenuating its effect. This behavior does not occur in the CT case, as the model in this scenario does not consider the interference coming from the specular direction.

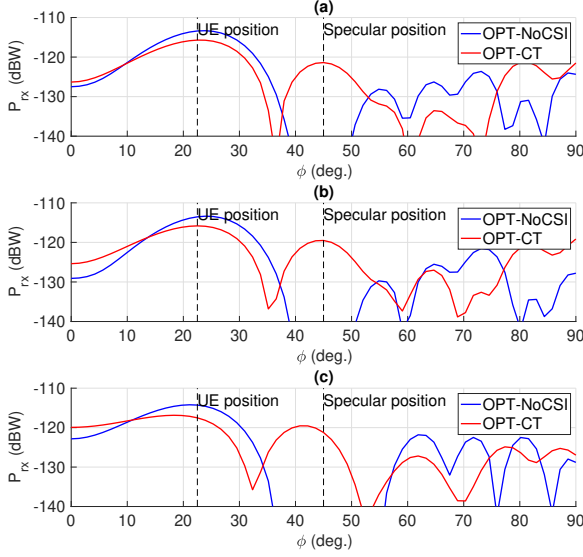


Fig. 11: Power received at the BS (in dBW) as a function of the angle  $\phi$  of the transmitting node for  $d_x = \lambda/4$  and the same setting as Fig. 10.

## VI. CONCLUSION

In this paper, we address the challenge of optimizing RISs for uplink communication systems in the presence of interfering users relying on statistical CSI. Specifically, our proposed approach utilizes knowledge of the channel correlation matrices to maximize the average achievable rate. To account for practical considerations often overlooked in traditional RIS models, we consider a MP network model that incorporates factors such as mutual coupling among scattering elements and the presence of structural scattering. Through simulations, we demonstrate the effectiveness of our approach, showing that in many cases, it manages to achieve performance reasonably close to the those achievable with perfect CSI. This is observed in scenarios where the uncertainty in the node position is small, e.g., 0.1 m and 0.5 m. In any case, the performance of the considered scheme is encouraging considering the significant reduction of RIS configuration overhead. Moreover, it is shown how in multi-user scenarios, namely in the presence of interference, the use of inadequate models to characterize RIS, which for example do not consider structural scattering, can lead to very poor performances due to the presence of interference caused by RIS not accounted for by the models.

## APPENDIX A – INTERPRETATION OF PROBLEM (16)

Let us denote by  $\mathbf{r} \in \mathbb{C}^{M \times 1}$  a random vector of i.i.d. zero mean uncorrelated Gaussian random variables with correlation  $\mathbf{R}_r = \mathbf{I}_M$ . Then, consider:

$$\tilde{\mathbf{y}} = \Phi \mathbf{U} \mathbf{D}^{1/2} \mathbf{r} + \Phi \sum_{i=2}^{N_u} \mathbf{w}_i + \mathbf{n}. \quad (48)$$

It's easy to verify that the function defined in (16) corresponds to the LMSE estimation of  $\mathbf{r}$  from  $\mathbf{v}^H \tilde{\mathbf{y}}$ , namely:

$$\mathcal{E}_r(\Lambda, \Phi, \mathbf{v}) = \mathbb{E} \left\{ \left\| \Lambda \mathbf{v}^H \tilde{\mathbf{y}} - \mathbf{r} \right\|^2 \right\} \quad (49)$$

where the average is computed with respect to all the random variables involved, namely, the channels and the noise and  $\Lambda \in \mathbb{C}^{M \times 1}$  is the linear filter. Accordingly, (17) is the optimal LMSE filter and (18) is the LMMSE.

## APPENDIX B – SOLUTION OF PROBLEM (22)

Introduce the terms:

$$\begin{aligned} \mathbf{R} &= \mathbf{R}_x + \sum_{i=2}^{N_u} R_{w_i} \\ C_1 &= 4Y_0^2 \mathbf{v}^H \mathbf{S} \mathbf{A}^{(k)} \mathbf{R} \left[ \mathbf{A}^{(k)} \right]^H \mathbf{S}^H \mathbf{v} \\ C_2 &= 4\sigma_n^2 Y_0^2 \mathbf{v}^H \mathbf{S} \mathbf{A}^{(k)} \mathbf{R} \mathbf{v} \\ \mathbf{d} &= -2Y_0 \mathbf{v}^H \mathbf{S} \mathbf{A}^{(k)} \mathbf{U} \mathbf{D}^{1/2} \end{aligned} \quad (50)$$

which allows us to reformulate the expression of  $Q$  and  $\mathbf{q}$  as:

$$\begin{aligned} Q &\approx C_1 + C_2 \\ &- 2\Re \left\{ 4Y_0^2 \mathbf{v}^H \mathbf{G}^{(k)} \text{diag}(\delta) \mathbf{A}^{(k)} \mathbf{R} \left[ \mathbf{A}^{(k)} \right]^H \mathbf{S}^H \mathbf{v} \right\} \\ &+ 4Y_0^2 \mathbf{v}^H \mathbf{G}^{(k)} \text{diag}(\delta) \mathbf{A}^{(k)} \mathbf{R} \left[ \mathbf{A}^{(k)} \right]^H \text{diag}(\delta) \left[ \mathbf{G}^{(k)} \right]^H \mathbf{v} \\ \mathbf{q} &\approx \mathbf{d} + 2Y_0 \mathbf{v}^H \mathbf{G}^{(k)} \text{diag}(\delta) \mathbf{A}^{(k)} \mathbf{U} \mathbf{D}^{1/2}. \end{aligned} \quad (51)$$

It is now convenient to introduce the terms:

$$\begin{aligned} \mathbf{R}_A &= \mathbf{A}^{(k)} \mathbf{R} \left[ \mathbf{A}^{(k)} \right]^H \in \mathbb{C}^{M \times M} \\ \mathbf{f}_1 &= 4Y_0^2 \mathbf{v}^H \mathbf{G}^{(k)} \in \mathbb{C}^{1 \times M} \\ \mathbf{f}_2 &= \mathbf{R}_A \mathbf{S}^H \mathbf{v} \in \mathbb{C}^{M \times 1} \\ \mathbf{f}_3 &= \left[ \mathbf{G}^{(k)} \right]^H \mathbf{v} \in \mathbb{C}^{M \times 1} \\ \mathbf{f}_4 &= 2Y_0 \mathbf{v}^H \mathbf{G}^{(k)} \in \mathbb{C}^{1 \times M} \\ \mathbf{f}_5 &= \mathbf{A}^{(k)} \mathbf{U} \mathbf{D}^{1/2} \mathbf{A}^{(k+1)} \in \mathbb{C}^{M \times 1} \\ \mathbf{F}_1 &= \text{diag}(\mathbf{f}_1) \in \mathbb{C}^{M \times M} \\ \mathbf{F}_3 &= \text{diag}(\mathbf{f}_3) \in \mathbb{C}^{M \times M} \\ \mathbf{f}_{1,2} &= \mathbf{f}_1^T \odot \mathbf{f}_2 \in \mathbb{C}^{M \times 1} \\ \mathbf{f}_{4,5} &= \mathbf{f}_4^T \odot \mathbf{f}_5 \in \mathbb{C}^{M \times 1}. \end{aligned} \quad (52)$$

Accordingly, by considering only the terms in (24) that depend on the optimization variable  $\delta$ , we can approximate the MSE (24) as:

$$\begin{aligned} \hat{\mathcal{E}}_r \left( \mathbf{A}^{(k+1)}, \Phi(\delta), \mathbf{v} \right) &= \left\| \mathbf{A}^{(k+1)} \right\|^2 \delta \mathbf{F}_1 \mathbf{R} \mathbf{F}_3 \delta^T \\ &- 2\delta \left[ \left\| \mathbf{A}^{(k+1)} \right\|^2 \Re(\mathbf{f}_{1,2}) + \Re(\mathbf{f}_{4,5}) \right]. \end{aligned} \quad (53)$$



We are now in a position to define the problem for finding the optimal  $\delta$  as:

$$\begin{aligned} \delta^* &= \arg \min_{\delta} \hat{\mathcal{E}}_{\mathbf{r}} \left( \mathbf{\Lambda}^{(k+1)}, \Phi(\delta), \mathbf{v} \right) . \\ \text{s.t. } &\sum_{m=1}^M \delta_m^2 \theta_m^2 < \epsilon^2 \end{aligned} \quad (54)$$

The problem in (54) is now convex and can be easily solved in the Lagrangian domain. First, from (53) we derive the gradient of the Lagrangian:

$$\begin{aligned} \nabla_{\delta} \left[ \hat{\mathcal{E}}_{\mathbf{r}} \left( \mathbf{\Lambda}^{(k+1)}, \Phi(\delta), \mathbf{v} \right) + \mu \left( \sum_{m=1}^M \delta_m^2 \theta_m^2 - \epsilon^2 \right) \right] \\ = 2\delta \left\| \mathbf{\Lambda}^{(k+1)} \right\|^2 \Re(\mathbf{F}_1 \mathbf{R} \mathbf{F}_3) \\ - 2 \left\| \mathbf{\Lambda}^{(k+1)} \right\|^2 \Re(\mathbf{f}_{1,2}) - \Re(\mathbf{f}_{4,5}) + 2\delta \Psi \end{aligned} \quad (55)$$

where  $\mu > 0$  is a Lagrange multiplier and  $\Psi \in \mathbb{C}^{M \times 1}$  is a vector with entries  $\theta_m^2$ . Accordingly, denoting by  $\mathbf{M} = \left\| \mathbf{\Lambda}^{(k+1)} \right\|^2 \Re(\mathbf{F}_1 \mathbf{R} \mathbf{F}_3)$  and  $\mathbf{v} = \left\| \mathbf{\Lambda}^{(k+1)} \right\|^2 \Re(\mathbf{f}_{1,2}) + \Re(\mathbf{f}_{4,5})$ , we finally obtain:

$$\delta^* = [\mathbf{M} + \mu \times \text{diag}(\Psi)]^{-1} \mathbf{v} \quad (56)$$

where  $\mu$  is set to satisfy the constraint in (54).

## REFERENCES

- [1] M. Di Renzo, M. Debbah, D.-T. Phan-Huy, A. Zappone, M.-S. Alouini, C. Yuen, V. Sciancalepore, G. C. Alexandropoulos, J. Hoydis, H. Gacanin, J. de Rosny, A. Bounceur, G. Lerosey, and M. Fink, "Smart radio environments empowered by reconfigurable AI meta-surfaces: an idea whose time has come," *EURASIP Journal on Wireless Communications and Networking*, vol. 2019, no. 1, pp. 1–20, 2019.
- [2] Q. Wu, S. Zhang, B. Zheng, C. You, and R. Zhang, "Intelligent reflecting surface-aided wireless communications: A tutorial," *IEEE Transactions on Communications*, vol. 69, no. 5, pp. 3313–3351, 2021.
- [3] M. Di Renzo, A. Zappone, M. Debbah, M.-S. Alouini, C. Yuen, J. de Rosny, and S. Tretyakov, "Smart radio environments empowered by reconfigurable intelligent surfaces: How it works, state of research, and the road ahead," *IEEE Journal on Selected Areas in Communications*, vol. 38, no. 11, pp. 2450–2525, 2020.
- [4] L. Venturino, N. Prasad, and X. Wang, "Coordinated linear beamforming in downlink multi-cell wireless networks," *IEEE Transactions on Wireless Communications*, vol. 9, no. 4, pp. 1451–1461, 2010.
- [5] H. Dahrouj and W. Yu, "Coordinated beamforming for the multicell multi-antenna wireless system," *IEEE Transactions on Wireless Communications*, vol. 9, no. 5, pp. 1748–1759, 2010.
- [6] Y. Sun, Z. Ding, X. Dai, and O. A. Dobie, "On the performance of network noma in uplink comp systems: A stochastic geometry approach," *IEEE Transactions on Communications*, vol. 67, no. 7, pp. 5084–5098, 2019.
- [7] Y. Sun, Z. Ding, and X. Dai, "A user-centric cooperative scheme for uav-assisted wireless networks in malfunction areas," *IEEE Transactions on Communications*, vol. 67, no. 12, pp. 8786–8800, 2019.
- [8] X. Wei, D. Shen, and L. Dai, "Channel estimation for ris assisted wireless communications—part i: Fundamentals, solutions, and future opportunities," *IEEE Communications Letters*, vol. 25, no. 5, pp. 1398–1402, 2021.
- [9] T. Demir and E. Björnson, "Is channel estimation necessary to select phase-shifts for ris-assisted massive mimo?" *IEEE Transactions on Wireless Communications*, vol. 21, no. 11, pp. 9537–9552, 2022.
- [10] T. Demir, E. Björnson, and L. Sanguinetti, "Exploiting array geometry for reduced-subspace channel estimation in ris-aided communications," in *2022 IEEE 12th Sensor Array and Multichannel Signal Processing Workshop (SAM)*, 2022, pp. 455–459.
- [11] M. Di Renzo, F. H. Danufane, and S. Tretyakov, "Communication models for reconfigurable intelligent surfaces: From surface electromagnetics to wireless networks optimization," *Proceedings of the IEEE*, vol. 110, no. 9, pp. 1164–1209, 2022.
- [12] S. Abeywickrama, R. Zhang, Q. Wu, and C. Yuen, "Intelligent reflecting surface: Practical phase shift model and beamforming optimization," *IEEE Transactions on Communications*, vol. 68, no. 9, pp. 5849–5863, 2020.
- [13] A. Rafique, N. Ul Hassan, M. Zubair, I. H. Naqvi, M. Q. Mehmood, M. D. Renzo, M. Debbah, and C. Yuen, "Reconfigurable intelligent surfaces: Interplay of unit cell and surface-level design and performance under quantifiable benchmarks," *IEEE Open Journal of the Communications Society*, vol. 4, pp. 1583–1599, 2023.
- [14] M. T. Ivrlač and J. A. Nossek, "Toward a circuit theory of communication," *IEEE Transactions on Circuits and Systems I: Regular Papers*, vol. 57, no. 7, pp. 1663–1683, 2010.
- [15] G. Gradoni and M. Di Renzo, "End-to-end mutual coupling aware communication model for reconfigurable intelligent surfaces: An electromagnetic-compliant approach based on mutual impedances," *IEEE Wireless Communications Letters*, vol. 10, no. 5, pp. 938–942, 2021.
- [16] X. Qian and M. D. Renzo, "Mutual coupling and unit cell aware optimization for reconfigurable intelligent surfaces," *IEEE Wireless Communications Letters*, vol. 10, no. 6, pp. 1183–1187, 2021.
- [17] A. Abrardo, D. Dardari, M. Di Renzo, and X. Qian, "Mimo interference channels assisted by reconfigurable intelligent surfaces: Mutual coupling aware sum-rate optimization based on a mutual impedance channel model," *IEEE Wireless Communications Letters*, vol. 10, no. 12, pp. 2624–2628, 2021.
- [18] M. Di Renzo, A. Zappone, M. Debbah, M.-S. Alouini, C. Yuen, J. de Rosny, and S. Tretyakov, "Smart radio environments empowered by reconfigurable intelligent surfaces: How it works, state of research, and the road ahead," *IEEE Journal on Selected Areas in Communications*, vol. 38, no. 11, pp. 2450–2525, 2020.
- [19] M. Movahediqomi, G. Puitcyn, and S. Tretyakov, "Comparison between different designs and realizations of anomalous reflectors for extreme deflections," *IEEE Transactions on Antennas and Propagation*, vol. 71, no. 10, pp. 8007–8017, 2023.
- [20] A. Abrardo, A. Toccafondi, and M. D. Renzo, "Analysis and optimization of reconfigurable intelligent surfaces based on s-parameters multiport network theory," *arXiv:2308.16856 [cs.IT]*, accepted in *IEEE EUCAP 2024*, August 2023.
- [21] —, "Design of reconfigurable intelligent surfaces by using s-parameter multiport network theory – optimization and full-wave validation," *arXiv:2311.06648 [cs.IT]*, November 2023.
- [22] X. Wei, D. Shen, and L. Dai, "Channel estimation for ris assisted wireless communications—part ii: An improved solution based on double-structured sparsity," *IEEE Communications Letters*, vol. 25, no. 5, pp. 1403–1407, 2021.
- [23] G. Zhou, C. Pan, H. Ren, P. Popovski, and A. L. Swindlehurst, "Channel estimation for ris-aided multiuser millimeter-wave systems," *IEEE Transactions on Signal Processing*, vol. 70, pp. 1478–1492, 2022.
- [24] T. L. Jensen and E. De Carvalho, "An optimal channel estimation scheme for intelligent reflecting surfaces based on a minimum variance unbiased estimator," in *ICASSP 2020 - 2020 IEEE International Conference on Acoustics, Speech and Signal Processing (ICASSP)*, 2020, pp. 5000–5004.
- [25] J. Chen, Y.-C. Liang, H. V. Cheng, and W. Yu, "Channel estimation for reconfigurable intelligent surface aided multi-user mmwave mimo systems," *IEEE Transactions on Wireless Communications*, vol. 22, no. 10, pp. 6853–6869, 2023.
- [26] A. de Jesus Torres, L. Sanguinetti, and E. Björnson, "Electromagnetic interference in ris-aided communications," *IEEE Wireless Communications Letters*, vol. 11, no. 4, pp. 668–672, 2022.
- [27] W.-X. Long, M. Moretti, L. Sanguinetti, and R. Chen, "Channel estimation in ris-aided communications with interference," *IEEE Wireless Communications Letters*, vol. 12, no. 10, pp. 1751–1755, 2023.
- [28] A. Abrardo, D. Dardari, and M. Di Renzo, "Intelligent reflecting surfaces: Sum-rate optimization based on statistical position information," *IEEE Transactions on Communications*, vol. 69, no. 10, pp. 7121–7136, 2021.
- [29] A. Zappone, M. Di Renzo, F. Shams, X. Qian, and M. Debbah, "Overhead-aware design of reconfigurable intelligent surfaces in smart radio environments," *IEEE Transactions on Wireless Communications*, vol. 20, no. 1, pp. 126–141, 2021.
- [30] M.-M. Zhao, Q. Wu, M.-J. Zhao, and R. Zhang, "Intelligent reflecting surface enhanced wireless networks: Two-timescale beamforming op-

- timization," *IEEE Transactions on Wireless Communications*, vol. 20, no. 1, pp. 2–17, 2021.
- [31] F. Jiang, A. Abrardo, K. Keykhosravi, H. Wymeersch, D. Dardari, and M. Di Renzo, "Two-timescale transmission design and ris optimization for integrated localization and communications," *IEEE Transactions on Wireless Communications*, vol. 22, no. 12, pp. 8587–8602, 2023.
  - [32] Q.-U.-A. Nadeem, A. Chaaban, and M. Debbah, "Opportunistic beamforming using an intelligent reflecting surface without instantaneous csi," *IEEE Wireless Communications Letters*, vol. 10, no. 1, pp. 146–150, 2021.
  - [33] Z. Peng, T. Li, C. Pan, H. Ren, W. Xu, and M. D. Renzo, "Analysis and optimization for ris-aided multi-pair communications relying on statistical csi," *IEEE Transactions on Vehicular Technology*, vol. 70, no. 4, pp. 3897–3901, 2021.
  - [34] N. S. Perović, L.-N. Tran, M. Di Renzo, and M. F. Flanagan, "Achievable rate optimization for mimo systems with reconfigurable intelligent surfaces," *IEEE Transactions on Wireless Communications*, vol. 20, no. 6, pp. 3865–3882, 2021.
  - [35] T. Van Chien, H. Q. Ngo, S. Chatzinotas, M. Di Renzo, and B. Ottersten, "Reconfigurable intelligent surface-assisted cell-free massive mimo systems over spatially-correlated channels," *IEEE Transactions on Wireless Communications*, vol. 21, no. 7, pp. 5106–5128, 2022.
  - [36] J. Hoydis, S. ten Brink, and M. Debbah, "Massive mimo in the ul/dl of cellular networks: How many antennas do we need?" *IEEE Journal on Selected Areas in Communications*, vol. 31, no. 2, pp. 160–171, 2013.
  - [37] M. McKay and I. Collings, "General capacity bounds for spatially correlated rician mimo channels," *IEEE Transactions on Information Theory*, vol. 51, no. 9, pp. 3121–3145, 2005.
  - [38] S. Shen, B. Clerckx, and R. Murch, "Modeling and architecture design of reconfigurable intelligent surfaces using scattering parameter network analysis," *IEEE Transactions on Wireless Communications*, vol. 21, no. 2, pp. 1229–1243, 2022.
  - [39] T. Demir, E. Björnson, and L. Sanguinetti, "Channel modeling and channel estimation for holographic massive mimo with planar arrays," *IEEE Wireless Communications Letters*, vol. 11, no. 5, pp. 997–1001, 2022.
  - [40] E. Björnson and L. Sanguinetti, "Rayleigh fading modeling and channel hardening for reconfigurable intelligent surfaces," *IEEE Wireless Communications Letters*, vol. 10, no. 4, pp. 830–834, 2021.